Petroleum Science 23 (2026) 2937–2949

Contents lists available at ScienceDirect

Petroleum Science

journal homepage: www.keaipublishing.com/en/journals/petroleum-science

Original Paper

Molecular insights into asphaltene desorption from silica surface by ionic and non-ionic nitrogen-based additives

Xue-Qian Liu [a,b,1], Chang-Qing He [a,b,1], Guo-Qiang Ma [c], Lin He [a,b,*], Hong Sui [a,b]

[a] School of Chemical Engineering and Technology, Tianjin University, Tianjin, 300072, China
[b] National Engineering Research Centre of Distillation Technology, Tianjin, 300072, China
[c] Tianjin Research Institute for Water Transport Engineering, M.O.T., Tianjin, 300456, China

ARTICLE INFO

Article history:
Received 23 April 2025
Received in revised form
3 November 2025
Accepted 28 January 2026
Available online 31 January 2026

Edited by Min Li

Keywords:
Asphaltene
Nitrogen-based additives
Desorption
Interfacial interactions
Molecular dynamics
Density functional theory

ABSTRACT

The strong adsorption of asphaltenes on reservoir minerals is a major constraint on heavy oil recovery. Although some nitrogen-based chemicals have shown promise in desorbing asphaltenes, their working mechanisms remain poorly understood. Herein, molecular dynamics (MD) and density functional theory (DFT) have been used to reveal the molecular-interaction mechanisms by which ionic liquids (ILc) and switchable-hydrophilicity solvents (in neutral (SHSn) and dicationic (SHSc) forms) facilitate asphaltenes desorption from silica surface. We identify two key functions of these nitrogen-based additives in enhancing the asphaltene desorption: (i) the nitrogen groups attack the asphaltene aggregates, reconstructing the hydrogen bonding between asphaltene molecules and dispersing the asphaltene aggregates through an encapsulation effect, and (ii) replacing the asphaltenes by competitive adsorption on solid surface. In particular, ILc significantly reduces asphaltene–silica interactions via charge complementarity, while SHSn displaces asphaltenes through hydrogen bonding yet displays limited efficacy, and SHSc exhibits strong electrostatic binding while favoring encapsulation, thereby constraining overall dispersion. Overall, nitrogen functionalities amplify electrostatic attraction and help overcome exchange-repulsion, suggesting that optimizing both dispersion and interfacial displacement will improve oil–solid separation. These mechanistic insights provide a foundation for the rational design of advanced nitrogen-based additives for enhanced heavy oil recovery and sustainable separation processes.

1. Introduction

Heavy oil components, particularly asphaltenes, readily adsorb onto mineral surfaces, making them difficult to be liberated and creating a host of bottlenecks in oil recovery. These obstacles not only reduce the oil recovery, but also lead to the entrapment of fine solids to the oil phase, all of which undermine the efficiency of separation, transportation and refining processes (Bastami et al., 2024; Liu et al., 2020). In oil–solid systems, the strong interactions between asphaltene molecules and mineral surfaces further complicate separation efforts (Gonzalez and Taylor, 2016; Lu et al., 2021; Yang et al., 2022). This highlights the need to understand their adsorption mechanisms and develop strategies to disrupt these interactions for more efficient resource extraction (Tazikeh et al., 2022).

Recent advances in oil–solid separation processes encompass a wide range of techniques, including thermal methods (Pratama and Babadagli, 2022), solvent-based extractions (Natarajan et al., 2014), chemical flooding (Dang et al., 2018; Razavinezhad et al., 2022), and microbial methods (Niu et al., 2020; Zhang et al., 2020). Despite proving effective under certain conditions, conventional methods often suffer from high energy consumption, considerable costs, or an inability to sufficiently disrupt the strong asphaltene adsorption on mineral surfaces (Ahmadi and Chen, 2020; Tazikeh et al., 2022). Recent experimental interrogation of asphaltene–sand mineral interfaces further highlights the strength and persistence of these interfacial interactions (Taheri-Shakib

* Corresponding author.
E-mail address: linhe@tju.edu.cn (L. He).
Peer review under the responsibility of China University of Petroleum (Beijing).
[1] These two authors contributed equally to this work.

https://doi.org/10.1016/j.petsci.2026.01.048

et al., 2024). Against this backdrop, the use of chemical additives has emerged as a promising strategy to break the strong adsorption bonds between asphaltenes and solids (Mohammed et al., 2024; Vatti et al., 2024). By directly targeting the interfacial properties between oil and mineral surfaces, additives facilitate the detachment and extraction of asphaltenes, thereby enhancing oil recovery efficiency (Melendez-Alvarez et al., 2016), while potentially offering a more economical and environmentally sustainable alternative to traditional techniques (Stratiev et al., 2025). In parallel, mobility-control approaches such as lignin-based foam stabilization provide broader EOR context in which interfacial strategies can be integrated (Saeedi Dehaghani and Behnam Motlagh, 2025).

Our previous results have demonstrated that incorporating nitrogen-based additives, particularly ionic liquids and CO_2 triggered switchable-hydrophilicity solvents, significantly enhances heavy oil/bitumen separation from mineral solid surfaces. Asphaltenes adsorb onto silica surfaces in compact monolayers, as confirmed by adsorption isotherms and AFM/QCM-D measurements. Disrupting this adsorption is key to improving separation efficiency (Zhang et al., 2023). For instance, a diamine-based switchable-hydrophilicity solvents increased heavy oil recovery from approximately 63%–96% in the presence of 30 vol% water (Li et al., 2018) whereas a low-viscosity imidazolium ionic liquid enabled bitumen extraction yields of about 95% under ambient conditions (Li et al., 2011). Likewise, a deep eutectic solvent derived from amino acid ionic liquids formed microemulsions that reached about 93% oil recovery, compared to 81% using conventional solvents (Zhang et al., 2018). In previous work, switchable-hydrophilicity tertiary amines were shown to enhance bitumen recovery by modifying bitumen–solid interfacial attributes (Sui et al., 2016), where further study by sum frequency generation (SFG) showed that the hydrophilic ionic liquid intensify the ordering of water near mineral surfaces and diminish bitumen–silica adhesion (Sui et al., 2018). Furthermore, simulation results suggest that ionic liquid molecules adsorb onto silica more strongly than the oil components, effectively displacing bitumen into the solvent (Li et al., 2016). Acting as surface-active agents at oil–water interfaces, these additives also reduce interfacial tension and facilitate heavy oil emulsification or dissolution, thereby expediting oil detachment (Li et al., 2018). Despite their substantial efficacy, however, the precise molecular mechanisms by which these additives operate remain poorly understood. This gap underscores the need for MD simulations and DFT calculations to elucidate the underlying atomic-scale interactions, ultimately guiding the design of even more effective oil–solid separation agents.

MD simulations and DFT quantum chemistry calculations have increasingly been employed to investigate these oil–solid interactions at both the microscopic and quantum levels. Recent studies indicate that the adsorption of asphaltenes on solid surfaces is mainly governed by electrostatic interactions (i.e. hydrogen bonds) and dispersion effect (i.e. Van der Waals forces). The properties are determined by the large organic molecular structure and the characteristics of the functional groups contained within the asphaltene. He et al. found that the driving force for the formation of electrostatic interactions is the electrostatic complementarity (He et al., 2022). The functional groups present in asphaltene interact with hydroxyl or charged sites located on the hydrophilic solid surface through hydrogen bonds or electrostatic adsorption. Fused aromatic hydrocarbons and alkyl chain structures in asphaltene exhibit a preference for interacting via dispersion effect with solid surfaces, particularly hydrophobic ones. Therefore, they enhance the stability of their adsorption conformation. Liu et al. (2019) showed that the polar groups present in asphaltenes, including carboxylic groups, establish hydrogen bonds with the surface –OH groups on quartz. This interaction leads to a high adsorption mass of 114 ng/cm^2. Adsorption on hydrophobic surfaces relies mainly on Van der Waals forces, characterized by their weak and low-density nature (62 ng/cm^2). The conclusions mentioned above are corroborated by the results from MD simulation, quartz crystal microbalance with dissipation monitoring (QCM-D) and atomic force microscope (AFM) (Xiong et al., 2017). Some studies have examined the fundamental mechanisms by which various additives (i.e. CO_2, surfactants, and nanoparticles) improve the separation of oil from solid surface. The fundamental mechanism involves the restructuring of the interactions within asphaltene–solid system. For conventional small molecule and organic polymer additives, their main mechanisms of action include dispersing asphaltene (Celia-Silva et al., 2020) and competitive adsorption (Fu et al., 2022). Nanoparticles are subjected to the significant influence of spatial hindrance effects (Zhou et al., 2024). However, current simulation approaches have not been applied to unravel the molecular interaction mechanisms of nitrogen-based materials in oil–solid separation processes. The lack of atomistic-level insights into how nitrogen-containing functional groups modulate interfacial interactions represents a critical knowledge gap that necessitates systematic exploration through combined MD simulations and DFT calculations.

To address this gap, we present a comprehensive multiscale simulation strategy that combines MD with DFT to dissect the interfacial roles of ionic and non-ionic nitrogen-based additives. The detailed purposes of this work are to: (i) understand the exact molecular interactions between nitrogen-based chemicals and asphaltenes/mineral surface; (ii) find the difference in the roles of different nitrogen-based chemicals (ionic and non-ionic) in dispersing and desorbing asphaltenes; (iii) provide fundamental knowledge and universal strategy of developing advanced functional materials for efficient solid–heavy oil separation. The overall research methodology is illustrated in Fig. 1. This combined MD/DFT approach not only achieves atomistic-level mechanistic insight previously inaccessible to experiments but also establishes a predictive paradigm for designing more effective oil–solid separation additives.

2. Methodology

2.1. MD simulation

2.1.1. Molecular models

As asphaltenes play a critical role in determining the efficiency of oil–solid separation (Hou et al., 2021; Montoya et al., 2014), an asphaltene model has been therefore constructed as the main functional component for simulation. This model was developed using experimental techniques such as elemental analysis (EA), MALDI-TOF MS, FTIR, XPS, and ^{1}H NMR, combined with an improved Brown–Ladner (B–L) method. As shown in Supporting Information S1, the resulting asphaltene has an average molecular weight of 1228.87, with a representative monomeric formula of $C_{80}H_{93}NO_2S_4$, and its average molecular structure is depicted in Table 1. Herein, two previously-investigated nitrogen-based additives were selected: 1-ethyl-3-methyl imidazolium tetrafluoroborate (ILc) (a low-viscosity ionic liquid (Li et al., 2011)) and N,N,N′,N'-tetraethyl-1,3-propanediamine (a switchable-hydrophilicity solvent featuring a diamine structure) (Li et al., 2018; Yang et al., 2021). Notably, switchable-hydrophilicity solvents can exist in either a neutral form (SHSn) or a dicationic form (SHSc), shown in Table 1.

For these molecules, the initial structural models were constructed using the Materials Studio (MS) software, followed by

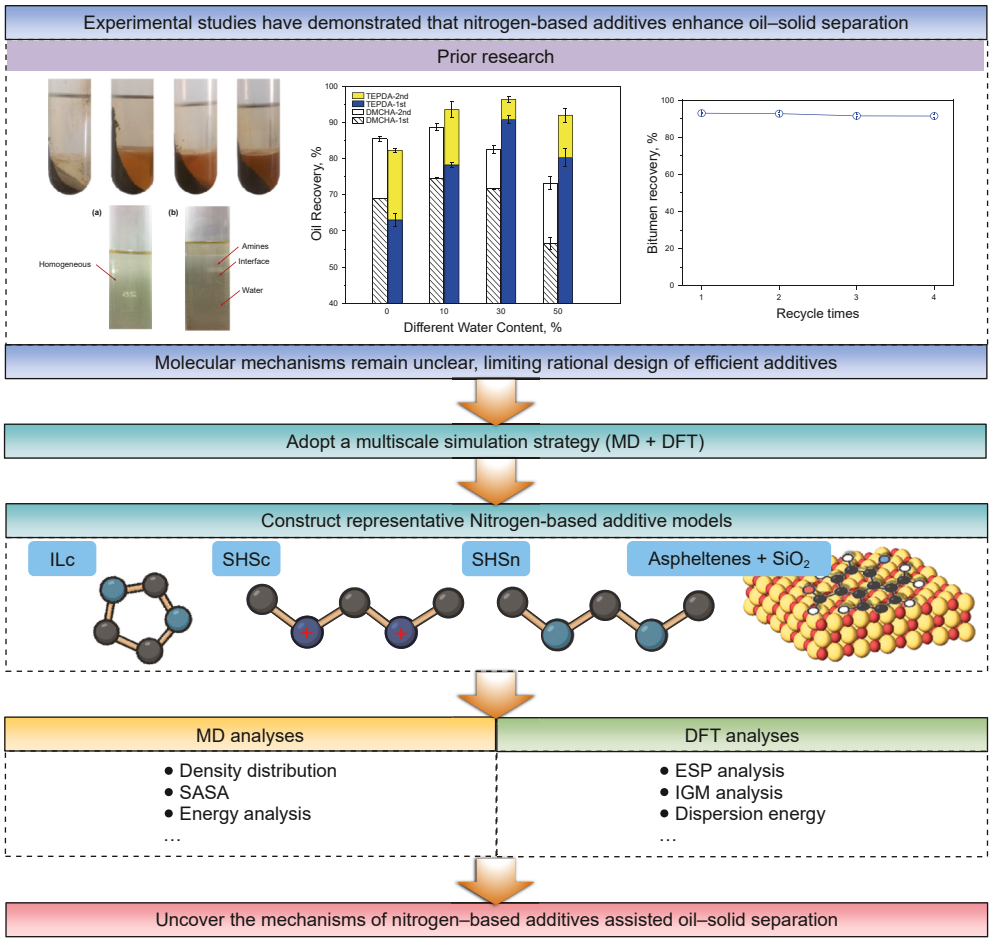

Fig. 1. Research framework based on our previous experimental studies. Reproduced with permission from Li et al. (2016) Copyright 2016, American Chemical Society; Li et al. (2018) with permission of Elsevier; Sui et al. (2016) with permission of Elsevier; Zhang et al. (2018) with permission of Elsevier.

Table 1
Molecualr models in simulation system.

Molecular components	Molecular structure	Chemical formula
Asphaltene model	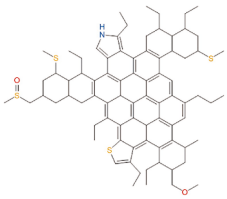	$C_{80}H_{93}NO_2S_4$
ILc	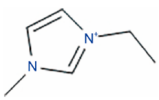	$C_6H_{11}N_2$
SHSn	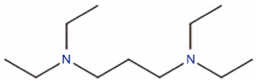	$C_{11}H_{26}N_2$
SHSc	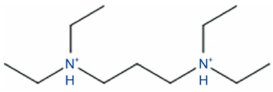	$C_{11}H_{28}N_2$

geometric optimization (Frisch et al., 2010). The sobtop_1.0 program (Lu, 2025) was then used to generate the initial topology files for all molecules. Subsequently, the Multiwfn 3.8 software (Lu and Chen, 2012) was employed to assign atomic charges, providing a more accurate description of electrostatic interactions among molecules.

2.1.2. Simulation systems

Before constructing the simulation models, two assumptions were made to ensure consistency. The SiO_2 surface was treated as a flexible surface to better capture interfacial interactions, and the additive concentrations were fixed according to experimentally validated dosages from our previous work. A silica surface model was constructed and preliminarily optimized using MS software. Specifically, the (0 1 0) surface of monoclinic α-quartz was chosen as the initial SiO_2 structure, and a supercell with the size of 7.9 nm × 9.8 nm × 2.3 nm was generated. Hydrogenation was then performed on the surface where each surface silicon atom was linked to two hydroxyl groups, yielding a grafting density of 7.54 OH/nm^2. The surface of SiO_2 was functionalized with hydroxyl groups (7.54 OH/nm^2). The contact angle of water on the surface of SiO_2 is 11.17°. This specific hydroxylation density corresponds to a fully hydroxylated SiO_2 surface, consistent with a hydrophilic surface. After hydrogenation, the hydroxyl structure underwent energy minimization to ensure its suitability and accuracy in subsequent MD simulations. After optimization, the geometry of surface hydroxyl groups was stabilized, enhancing both the realism and reliability of the SiO_2 surface model. The model of SiO_2 and the content related to its physical properties are shown in Supporting Information S2.

Next, six model asphaltene molecules were combined with the silica surface using the PACKMOL software (Martínez et al., 2009) to construct the initial MD simulation system. The asphaltene molecules were uniformly placed 1–3 nm above the silica surface, providing sufficient space for interactions and adsorption to occur once the simulation began. A preliminary 10 ns MD run was then conducted to allow the asphaltene molecules to fully adsorb onto the silica surface. The simulation results showed that all six asphaltene molecules successfully adhered to the silica surface, with the energy of the system stabilizing and the molecules packing closely without overlapping.

Based on the optimal additive ratios determined in previous experimental studies, the proportions of additives, asphaltenes, and solvents in the MD simulation systems were further refined to closely replicate the complex chemical environment encountered in oil–solid separation. The additive concentration in each system was fixed to match experimentally relevant dosages used in our prior work. As shown in Table 2, five distinct systems (ILS, ILA, RSS, RSN, and RST) were constructed to systematically investigate the roles of additive types and solvent environments in asphaltene adsorption and desorption.

As shown in Table 2, the ILS system provides a baseline for evaluating the inherent adsorption behavior of asphaltenes. Building on this, the ILA system incorporates additional ILc molecules, enabling an assessment of how these additives modulate asphaltene desorption. In parallel, the RSS system offers another pure solvent environment, serving as a control for comparative analysis, where the OPC3 water model was employed and all bond lengths involving hydrogen atoms were constrained using the LINCS algorithm. To further elucidate the effect of amine-based additives, the RSN system includes the nonionic variant SHSn, examining its ability to influence desorption pathways, while the RST system employs the dicationic form SHSc to ascertain how charge state affects the desorption mechanism. Through these five carefully designed systems, the relative contributions of solvent composition, ionic liquid additives, and additive charge state to the asphaltene adsorption–desorption process can be systematically characterized. Fig. 2 provides schematic representations of these five systems.

2.1.3. Simulation details

This study aims to investigate how nitrogen-based additives influence the desorption of asphaltenes adsorbed on a silica surface. To achieve this, the MD simulations were divided into two primary stages: (1) asphaltene adsorption onto the silica surface, and (2) the regulatory effect of additives on asphaltene desorption in five different systems. All simulation systems firstly underwent energy minimization using both the Conjugate Gradient method and the Steepest Descent method in alternating fashion, with a convergence criterion set at 100 kJ/(mol·nm). During this process, a flexible mode was adopted, allowing changes in molecular bonds, angles, and dihedrals while constraining the simulation box dimensions, thereby enabling a rapid shift toward a lower energy state and more stable molecular conformations. After completing the energy minimization, a 5 ns NPT ensemble equilibration was performed to eliminate any unstable initial conformations and reduce random fluctuations in the simulation results.

A GROMOS96 force field equipped with the 53A6 parameter set was employed (Oostenbrink et al., 2004), known for its robust performance in describing the interactions and conformations of polycyclic aromatic compounds (Bai et al., 2019; Kuznicki et al., 2009). The simulations were conducted at 300 K and 0.1 MPa under the NPT ensemble, using a timestep of 1 fs for a 20 ns production run. V-rescale and Berendsen coupling methods were used to stabilize temperature and pressure, respectively. Long-range electrostatic interactions were calculated via the PME algorithm, while short-range Van der Waals and electrostatic interactions were evaluated using a cutoff radius of 1.2 nm. Periodic boundary conditions were applied in all directions. Visual Molecular Dynamics (VMD) software was used to visualize molecular conformations and track system evolution (Humphrey et al., 1996). Additional analysis of potential energy stability, block-averaged interaction energies, and mean squared displacement (see Supporting Information S3) confirm that the simulations are well converged and free from kinetic trapping within the 20 ns production window.

To ensure statistical robustness, in addition to the original production run, two further independent simulations were performed for each system with different random velocity seeds and modified initial asphaltene positions. Detailed descriptions of these additional simulations are provided in Supporting Information S4.

Table 2
Composition of simulation systems.

System	Mole, %			
ILS	Asphaltene	Acetone	Heptane	
	0.23	39.97	59.80	
ILA	Asphaltene	Acetone	Heptane	ILc
	0.20	32.68	48.93	18.19
RSS	Asphaltene	H_2O		
	0.11	99.89		
RSN	Asphaltene	H_2O	SHSn	
	0.28	79.26	20.46	
RST	Asphaltene	H_2O	SHSc	
	0.28	79.66	20.06	

2.2. DFT quantum chemistry calculation

The non-covalent interactions within the additive-asphaltene system are categorized under quantum chemistry calculations, whereas those within the additive-SiO_2 system are categorized under first-principles calculations. In the subsequent sections, the distinctions between quantum chemistry and first principles will no longer be emphasized. They will be collectively referred to as DFT simulations.

2.2.1. Molecular models

To investigate the function of nitrogen elements, two models were constructed wherein nitrogen atoms were replaced with carbon atoms. These models consisted of carbon and hydrogen elements and were designated as IL-CH and SHS-CH, respectively. The molecular structures of IL-CH and SHS-CH were shown in Fig. 3. The ILc, SHSn, SHSc, and asphaltenes were consistent with those utilized in the MD simulations.

In a quartz crystal, the (0 1 0) crystal plane was focused. Subsequently, the unit cell was uniformly expanded by a factor of 4 along the *X*, *Y*, and *Z* axes. This resulted in the creation of a supercell with a volume 32 times larger than that of the original unit cell. The silicon hydroxyl group was originally located at the bottom position within the initial unit cell. The entire supercell was rotated by 180°, causing the surface with the silicon hydroxyl group to now face upwards. A vacuum layer was introduced in the *Z*-direction, and the overall height in the vertical direction was adjusted to 50 Å.

2.2.2. DFT simulations of additive–asphaltene systems

The calculations were performed using the Gaussian 09 software, and the analysis of the results was conducted using the Multiwfn 3.8 software. To optimize a system with limited

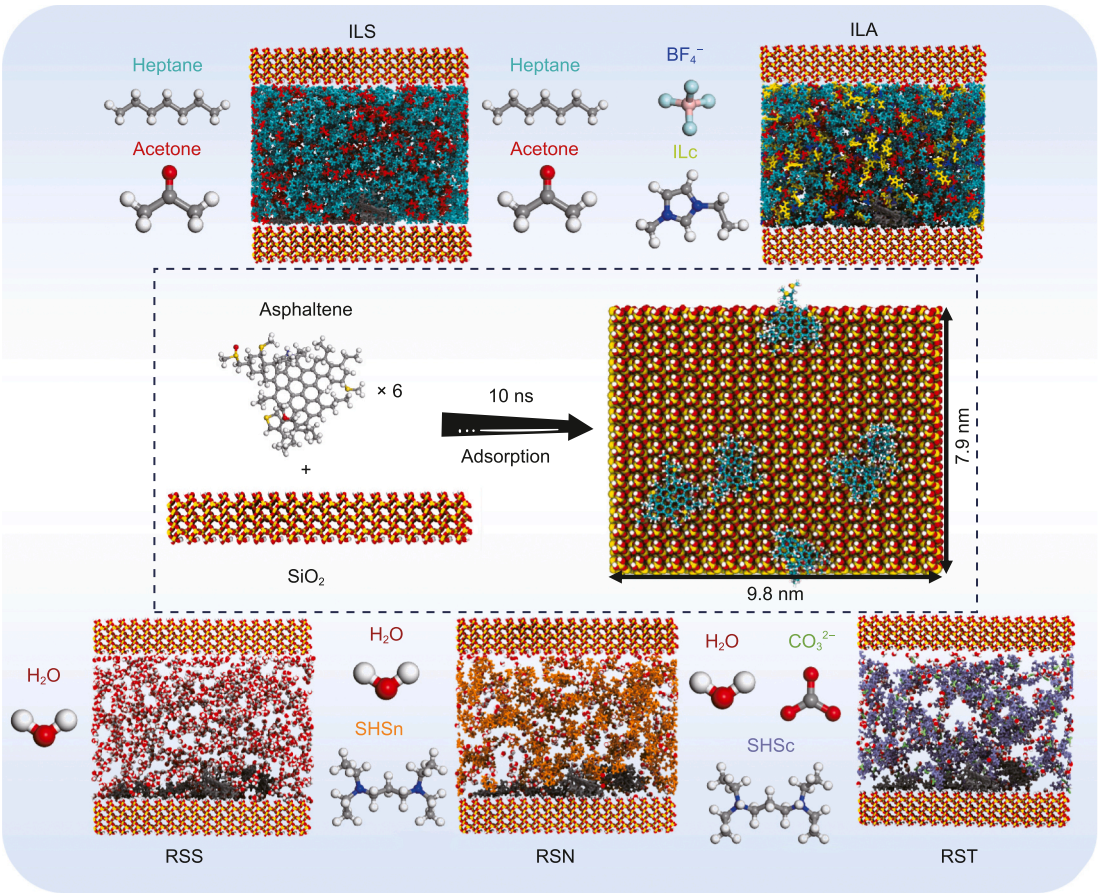

Fig. 2. Schematic of the MD simulation systems.

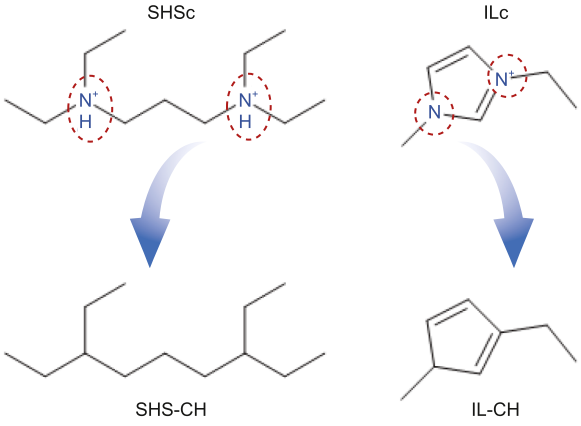

Fig. 3. SHS-CH and IL-CH models with carbon atoms replacing nitrogen atoms.

computing power, a multi-level optimization strategy was employed. Firstly, the initial structure was subjected to 5000 conformational searches using the Molclus software under the MMFF94 force field. Subsequently, the structure was subjected to semi-empirical geometric optimization utilizing the GFN2-xTB method (Lu and Chen, 2012). The structure was subsequently refined utilizing the B3LYP/6-31G(d) functional and basis set, with consideration given to the impact of dispersion correction (Bannwarth et al., 2019). After optimization, the conformation underwent single-point energy calculations utilizing the M062X/6-311+G (d, p) functional and basis set. The resulting wavefunction files were then employed for subsequent analysis and research. The principle of conformational search is detailed in the Supporting Information S5.

2.2.3. DFT simulations of additive–SiO_2 system

The calculations were performed utilizing the CP2k software (Burns et al., 2011), while the analysis outcomes were acquired via the Multiwfn 3.8 software. The initial conformation of the additive-SiO_2 system was as follows: a single additive molecule was positioned within the vacuum layer, ensuring that all atoms were contained within the lattice structure. The calculations relied on the lattice dimensions in the *X*, *Y*, and *Z* directions, with values of 21.6, 19.6, and 50.0 Å, respectively. This approach aimed to prevent energy changes caused by variations in lattice size. Initially, semi-empirical geometry optimization was performed using GFN1-xTB, with periodicity maintained in the *XY* directions and the SiO_2 surface fixed. Subsequent geometry optimization was conducted utilizing the PBE/DZVP-MOLOPT-SR-GTH functional and basis set, also retaining periodicity in the *XY* direction. Dispersion correction was applied throughout, with the SiO_2 surface being kept unfixed.

2.3. Calculation of properties

A comprehensive description of the methodologies, computational parameters, and analytical procedures employed for the calculation of all reported properties is provided in Supporting Information S6.

3. Results and discussions

3.1. Elucidation of asphaltene desorption behavior from silica surfaces

Extent of asphaltene desorption. In Fig. 4(a)–(e), the density distribution (along the *Z*-axis) is displayed alongside the final configurations, clearly illustrating the degree of asphaltene desorption in the five different systems. To more directly visualize asphaltene adsorption on the silica surface, solvent molecules were hidden in the structures, and the additive molecules were rendered in a "glass bubble" style, thereby highlighting the extent of asphaltene–silica interaction.

From Fig. 4(a) and (d), it is evident that in the ILS and RSS systems, asphaltene molecules exhibit pronounced adsorption behavior. They adhere firmly to the silica surface, forming a compact and relatively stable adsorbed layer. Specifically, in the ILS system, the asphaltene density reaches 360.77 kg/m^3 at 1.74 nm, whereas in the RSS system, the highest density of 348.85 kg/m^3 occurs at 1.86 nm. This suggests that pure solvent alone has limited capacity to detach asphaltene molecules, causing them to remain at their original adsorbed positions rather than being readily removed. Hence, it is insufficient to weaken the interaction between asphaltenes and the mineral surface solely relying on a pure solvent strategy.

A comparison of Fig. 4(a)–(c) reveals that in the RST system, asphaltenes have a peak density of 351.28 kg/m^3 at 2.06 nm, while in the RSN system, the highest density of 253.44 kg/m^3 is found at 3.35 nm. This result indicates that introducing nonionic SHSn into the RSN system not only pushes asphaltene molecules farther away from the silica surface in the vertical direction, thereby significantly enhancing desorption, but also partially displaces asphaltenes on the silica surface, which further weakens the asphaltene–silica surface interaction. By contrast, in the RST system, the dicationic SHSc exhibits stronger interactions with asphaltenes, tending to encapsulate the asphaltene molecules. Although the peak density shifts slightly relative to the RSS system, the high density observed shows that the asphaltene–solid surface interactions remain strong. Additionally, SHSc's encapsulation of asphaltenes partially preserves robust asphaltene–solid surface adsorption. Overall, these results demonstrate that the different charge states of the SHSn and SHSc additives lead to

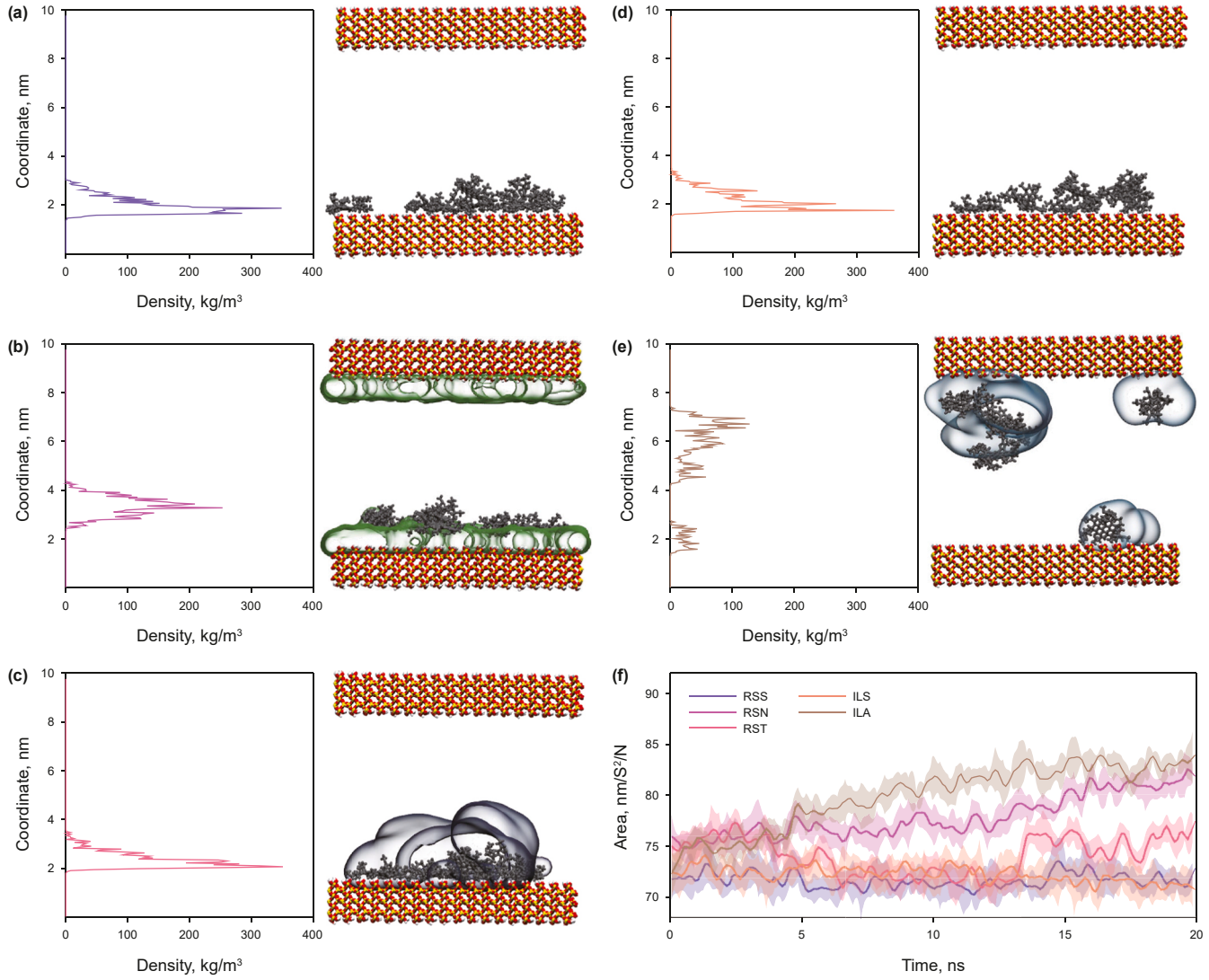

Fig. 4. Composite figure of final configurations and density distributions along the *Z*-axis for the five systems. **(a)** RSS; **(b)** RSN; **(c)** RST; **(d)** ILS; **(e)** ILA, and **(f)** SASA profiles across systems.

markedly different desorption outcomes: SHSn reduces the interaction between asphaltenes and the solid surface more effectively, whereas SHSc encloses asphaltene molecules, thereby sustaining stronger asphaltene–solid surface adsorption.

Fig. 4(d) and (e) illustrate the extent of asphaltene desorption in the ILS and ILA systems. It is evident that in the ILA system, the asphaltenes exhibit a higher degree of desorption and a broader spatial distribution, indicating that the added ILc effectively reduces the affinity between asphaltenes and the silica surface. This disruption facilitates the detachment and diffusion of asphaltenes from the solid surface. Compared with the ILS system, asphaltenes in the ILA system display a more dispersed spatial distribution. The definition and analysis of desorption extent provided in Supporting Information S4 further corroborate these observations.

SASA can be utilized to assess the amount of molecular surface area exposed to solvent molecules, thereby reflecting the dynamics of intermolecular interactions, shown in Fig. 4(f). Notably, in the ILA and RSN systems, the SASA of asphaltenes increases steadily over time, verifying that asphaltene molecules gradually detach from their initial adsorption sites and come into closer contact with surrounding solvent. Furthermore, the asphaltenes are able to depart from the solid surface more stably in the ILA system, whereas in the RSN system, SHSn primarily weakens the asphaltene–solid surface bond through competitive adsorption on the silica surface.

In comparison, the SASA profile of the RST system exhibits a different trend: in the early stage, the SASA value decreases noticeably, indicating a stronger interaction between dicationic SHSc and asphaltenes. This, in turn, partially shields the asphaltene surface from solvent, temporarily reducing the accessible surface area. However, as molecular conformations adjust along with the time, parts of the asphaltenes re-expose themselves to the solvent, causing the SASA to rise back to its initial level. This process suggests that although the dicationic additive in the RST system demonstrates a strong encapsulation or coupling effect during the initial adsorption stage, it does not sustain the same level of enhanced asphaltene desorption observed in the ILA or RSN systems.

Desorption of asphaltenes from mineral surface. Fig. 5(a) presents the interaction energies between asphaltenes and silica in each system, while Fig. 5(b) and (c) illustrate the temporal evolution of hydrogen bonds for the ILS/ILA systems and RSS/RSN/RST systems, respectively. This collective dataset enables a systematic evaluation of the distinct desorption behaviors observed across different systems and the underlying mechanisms governing these behaviors.

From Fig. 5(a), it is evident that the strength of asphaltene–silica binding varies significantly among the tested systems. The high negative values of their interaction energies suggest that the solvent environment alone does not sufficiently weaken the interactions between asphaltenes and silica. In contrast, significant reduction in interaction energies is observed in ILA, RSN, and RST, indicating that these additives effectively disrupt asphaltene–mineral binding and facilitate desorption. Notably, in the ILA system, the total interaction energy decreases from −1151.13 to −214.68 kJ/mol, while in the RSN system it decreases from −1222.09 to −502.34 kJ/mol. Such pronounced reduction implies that enhanced polar competition or solvation effects effectively diminish the hydrogen bonds and other intermolecular forces between asphaltenes and the solid surface.

In the RST system, the interaction energy shows only a moderate decline, reflecting a persistent asphaltene–solid surface adsorption. While some degree of desorption may occur, it appears to be partial or transient, making it difficult to achieve sustained or efficient asphaltene detachment in this specific environment.

Although hydrogen bonding is not the principal driving force governing asphaltene adsorption and desorption, it nonetheless serves as an important indicator at the microscopic scale, offering insights into the desorption mechanisms. Fig. 5(b) illustrates the evolution of hydrogen bond counts between asphaltenes and silica for the ILS and ILA systems. Fluctuations in both the magnitude and time dependence of these counts directly reflect the strength and dynamical stability of polar interactions between asphaltenes and the solid surface. In the ILS system, the hydrogen bond number increases over time with pronounced fluctuations, suggesting that asphaltenes maintain relatively strong and dynamic polar interactions with the solid surface. By contrast, in the ILA system, the hydrogen bond count shows a steady decline and eventually falls near zero by approximately 12 ns, clearly signifying a desorption process. The sustained disruption of hydrogen bonds demonstrates that IL–asphaltene interactions (via hydrogen bonding or ion–π forces) not only break the asphaltene–surface adhesion but also foster asphaltene–additive complexes, thus improving desorption.

Fig. 5(c) compares the hydrogen bond variation in the RSS, RSN, and RST systems. In the reversible solvent system RSS, the absence of an active additive restricts any significant reduction in hydrogen bonds, leaving the tight asphaltene–solid surface binding

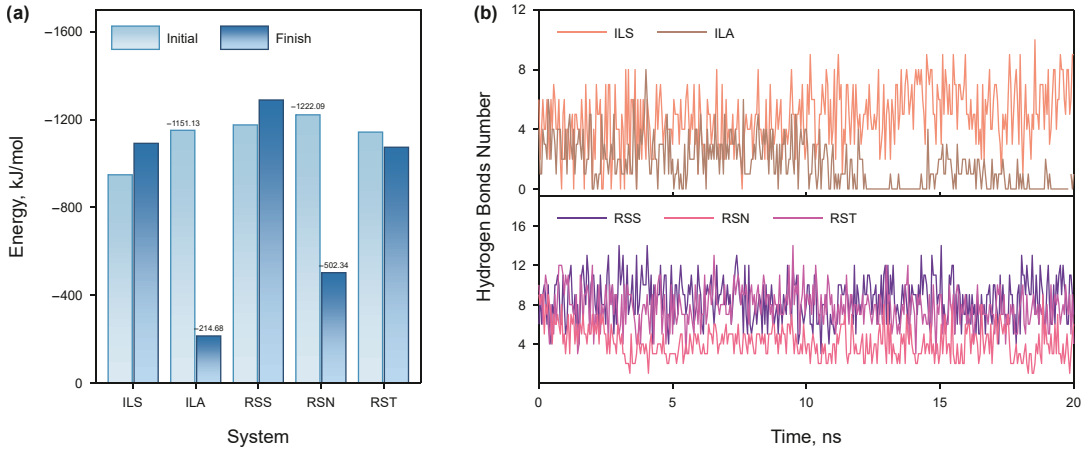

Fig. 5. **(a)** Total interaction energy between asphaltenes and silica in each system. **(b)** Temporal evolution of hydrogen bonds between asphaltenes and silica in the ILS and ILA systems. **(c)** Temporal evolution of hydrogen bonds between asphaltenes and silica in the RSS, RSN and RST systems.

essentially unaltered. In the RSN system, however, the introduction of nonionic SHSn maintains the hydrogen bond count at a relatively low level (2–5 bonds). It suggests that the additive effectively competes with asphaltenes for the active sites on silica, thereby reducing the probability of direct asphaltene–solid surface binding and fundamentally inhibiting the further formation of hydrogen bonds. The additive may also form weak aggregates or complexes with asphaltenes, which further attenuates their interaction with the solid surface. By contrast, although the dicationic SHSc in the RST system encapsulates asphaltenes at early stages, this disruptive effect on the asphaltene–solid surface interaction is not sustained, as evidenced by a resurgence of hydrogen bonds at later time, resulting in desorption efficiencies less pronounced than those observed in the RSN system.

3.2. Interfacial behavior of nitrogen-based additives

Fig. 6 displays the distribution of ESP on the surfaces of additives, asphaltene, and SiO_2 surface, along with a histogram illustrating the interval distribution of ESP on each molecular surface. As cations, ILc and SHSc have an overall positive ESP with values exceeding +292.88 kJ/mol, and their highest ESP values range from +627.60 to 836.80 kJ/mol. The neutral molecule SHSn has a negative ESP, with the lowest ESP value of the molecular surface reaching −133.43 kJ/mol. However, the electronegativity of the amine groups is inadequate to establish a significantly positive ESP region. The maximum ESP value on the molecular surface is merely +49.45 kJ/mol.

The molecular surfaces of asphaltene and SiO_2 surface exhibit ESP heterogeneity due to the presence of functional groups. The asphaltene contains functional groups such as sulfonyl, pyrrole, thiophene, ether, and thioether, which exhibit an ESP value ranging from −223.47 to +227.19 kJ/mol. Significantly, a wide negative ESP region has been developed within the fused ring area of asphaltene, and multiple points with extreme low ESP have emerged therein. For SiO_2 surface, the ESP demonstrates periodic distribution characteristics. The oxygen atoms within the silanol groups demonstrate a negative ESP on the molecular surface because of their electronegativity, whereas the hydrogen atoms within the silanol groups display a positive ESP.

Fig. 7 depicts the IGM analysis illustrating the interaction of various additive molecules with the asphaltene, displaying isosurface values of $\delta_g = 0.01$. The additives exhibit spatially extended green isosurfaces with the asphaltene molecule, indicating weak dispersion-dominated interactions. The cationic ILc and SHSc species continue to exhibit an attraction towards the fused ring region with a high negative ESP. This optimal conformation not only follows the principle of ESP complementarity, but also ensures a relatively large contact area between organic molecules. It facilitates the efficacy of Van der Waals forces. The amine groups in the SHSn molecule exhibit negative ESP, and the SHSn molecule surface lacks positive ESP regions. Therefore, the optimal conformation of the molecule exhibits a preference to interact with areas close to the side chains, rather than large fused ring regions.

The adsorption conformation of SHSn with asphaltene differs from those of ILc and SHSc with asphaltene. This indirectly impacts the interaction energy between additives and asphaltene. Table 3 illustrates the interaction energies between various additive molecules and asphaltenes, as well as the additives' respective contributions to dispersion energy. The total interaction energies for ILc–asphaltene (−199.07 kJ/mol) and SHSc–asphaltene (−357.27 kJ/mol) significantly surpass their corresponding dispersion energy components (−134.85 and −261.37 kJ/mol, respectively). The strong interactions between the two cations and asphaltene increase the stability and spontaneity of encapsulating asphaltene molecules. This observation aligns with the encapsulation behavior observed in the MD simulations. Since ILc molecules are small, they exhibit a minimal steric hindrance effect. Consequently, ILc demonstrates an effective dispersing role in asphaltene aggregates. The interaction energy between SHSn and asphaltene is −91.09 kJ/mol, which is much weaker than that of the dispersion energy (−212.05 kJ/mol). Thus, in MD simulations, SHSn exhibits a lack of tendency for encapsulating and dispersing asphaltenes.

Fig. 8 presents the SobEDAw decomposition results of interaction energies between different additives and asphaltenes. These energy contributions also serve as the driving forces of interactions in the process of MD simulations and the reflections of the final equilibrium results. Under the interactions of different physical mechanisms, the system gradually tends to be stable. Fig. 8 clearly demonstrates that the strongest attraction between additives and asphaltenes is dispersion attraction ΔE_{disp}, while the strongest repulsion is exchange-repulsion interaction ΔE_{xrep}. The absolute values of ΔE_{disp} and ΔE_{xrep} are remarkably close, with both being dependent on molecular size and intermolecular distance. ILc and SHSc exhibit significantly stronger electrostatic attraction than that of SHSn. This results from the mutual attraction between cations and the delocalized electrons in asphaltenes. ΔE_{orb} has a more significant influence on covalent bonds

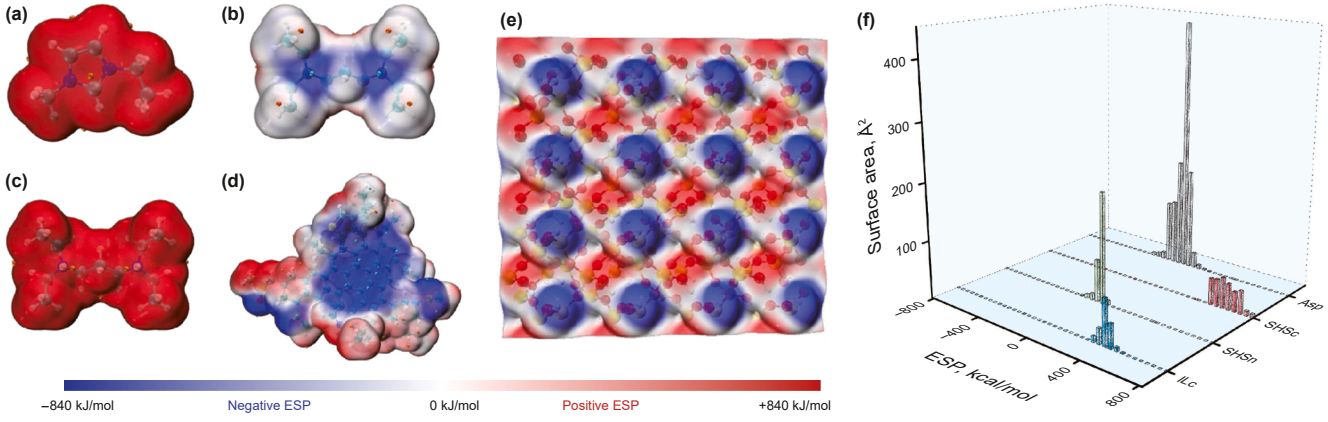

Fig. 6. The ESP at molecular surface of various molecules **(a)** ILc molecule, **(b)** SHSn molecule, **(c)** SHSc molecule, **(d)** asphaltene molecule, and **(e)** SiO_2 surface. **(f)** A histogram depicting the range distribution of ESP at molecular surface for each molecule.

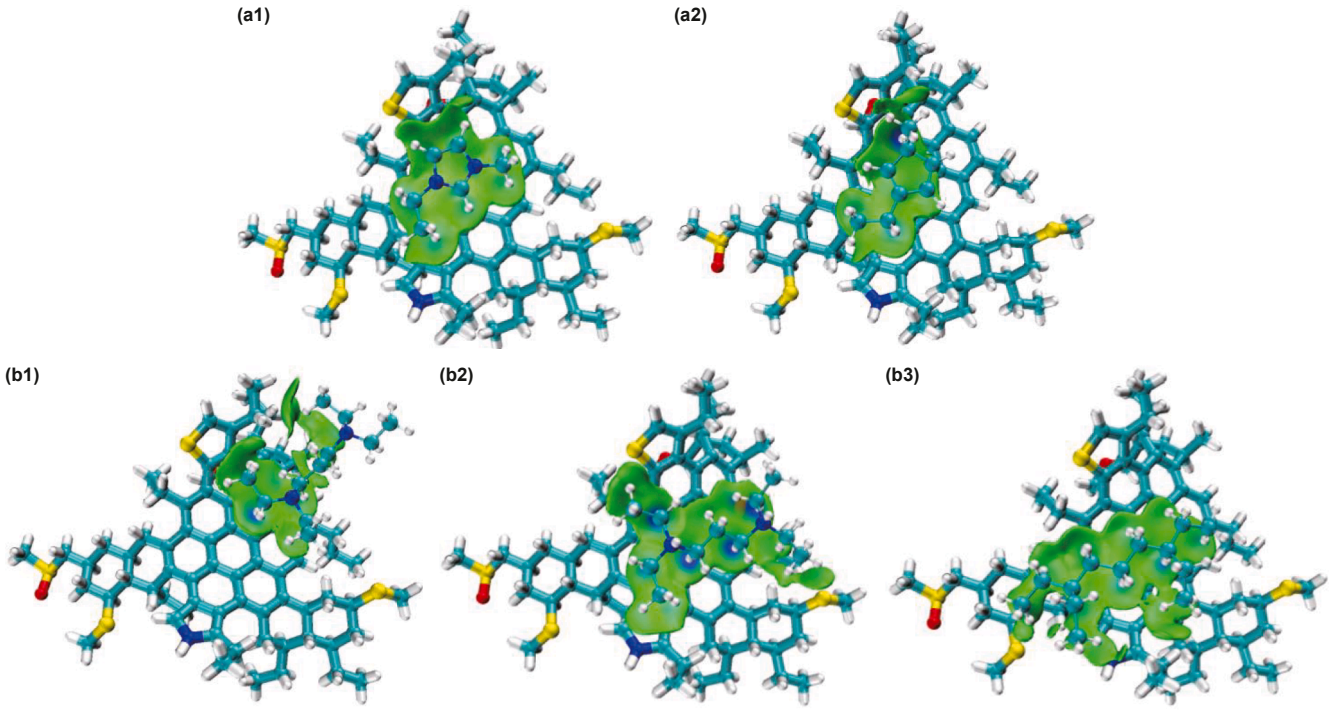

Fig. 7. IGM analysis of different additive molecules interacting with asphaltene: **(a1)** ILc molecule, **(a2)** IL-CH molecule, **(b1)** SHSc molecule, **(b2)** SHSn molecule, **(b3)** SHS-CH molecule.

Table 3
Interaction energies between various additive molecules and asphaltenes, and the corresponding contributions of additives to dispersion energy.

Additives	The interaction energies between various additive molecules and asphaltene, kJ/mol	Additives' respective contributions to dispersion energy, kJ/mol
ILc	−199.07	−134.85
IL-CH	−82.22	−133.89
SHSn	−91.09	−212.05
SHSc	−357.27	−261.37
SHS-CH	−125.27	−247.73

compared to non-covalent interactions. The effect of ΔE_{orb} on SHSn is minimal, whereas its impact on ILc and SHSc cannot be ignored. This indicates that the interaction between cations and asphaltenes already exhibits certain covalent characteristics.

The role of nitrogen atoms can be revealed through comparative analysis of IL-CbleH and SHS-CH. The IL-CH and SHS-CH molecules exhibit a tendency to adsorb within the fused aromatic ring region of asphaltene, resulting in the formation of an expanded region of Van der Waals force. Replacing nitrogen atoms with carbon atoms has little impact on the dispersion interaction. The electrostatic interactions of molecules consisting solely of carbon and hydrogen atoms can be ignored. Therefore, IL-CH and SHS-CH do not exhibit cationic electrostatic attraction, thus avoiding the electrostatic repulsion between SHSn's negative charge and the asphaltene's fused ring region. However, the impact of the exchange-exclusion interaction between IL-CH or SHS-CH and asphaltene is significant. The interaction exhibits a notably weak affinity, characterized by specific energies of −82.22 kJ/mol and −125.27 kJ/mol, respectively. The primary mechanism by which nitrogen atoms encapsulate and disperse asphaltene aggregates relying on electrostatic attraction and dispersion. The undissociated amine groups exhibit repulsive interactions with the fused ring structure of the asphaltene, thereby impairing their affinity for the asphaltenes and leading to negative consequences.

Table 4 demonstrates that the interactions between asphaltene and additives are significantly influenced by solvents. The absolute value of $\Delta\Delta G$ is extremely high and shows strong dependence on

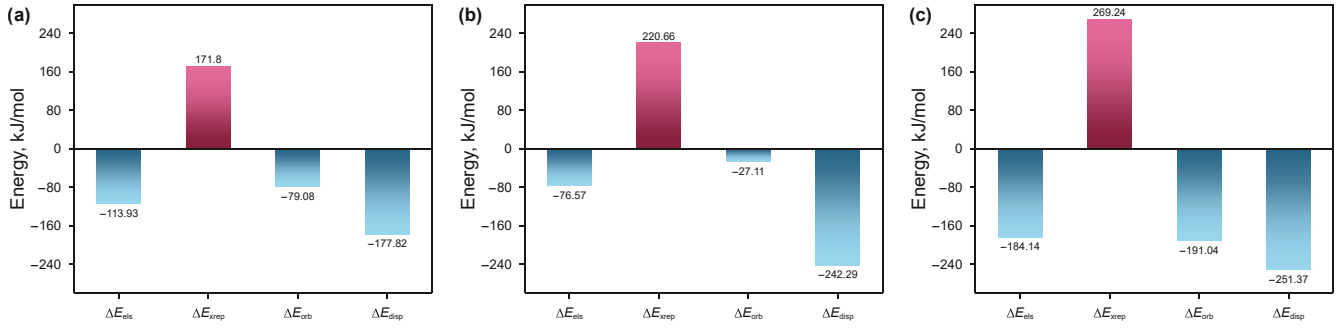

Fig. 8. SobEDAw decomposition results of interaction energies between different additives and asphaltene: **(a)** ILc, **(b)** SHSn, **(c)** SHSc.

Table 4
Interaction energies between various additive molecules and asphaltenes within different implicit solvents.

	Vacuum	Acetone		Heptane		Water	
	ΔE, kJ/mol	ΔE_{solv}, kJ/mol	$\Delta\Delta G_{solv}$, kJ/mol	ΔE_{solv}, kJ/mol	$\Delta\Delta G_{solv}$, kJ/mol	ΔE_{solv}, kJ/mol	$\Delta\Delta G_{solv}$, kJ/mol
ILc	−199.07	−319.20	−120.12	−552.50	−353.42	/	/
IL-CH	−82.22	−267.23	−185.02	−254.01	−171.80	/	/
SHSn	−91.09	/	/	/	/	−386.48	−295.39
SHSc	−357.27	/	/	/	/	−506.39	−149.12

the types of both additives and solvents. Nonpolar solvents (i.e., heptane) lead to higher absolute values of $\Delta\Delta G_{solv}$ (−353.42 kJ/mol) for polar additives (i.e., ILc). Correspondingly, polar solvents (i.e., water) lead to higher absolute values of $\Delta\Delta G_{solv}$ (−295.39 kJ/mol) for weakly polar additives (i.e., SHSn). The principle of hydrophobic effect can well explain these phenomena. Acetone, heptane, and water are all poor solvents for asphaltenes, since asphaltenes can only be well dissolved in aromatic hydrocarbons, such as toluene. Therefore, when the solvent is a poor solvent for the additive, the additive exhibits sustained association with asphaltenes. This reduces the contact area between the additive/asphaltene and solvent, consequently increasing entropy. Under the premise of good additive dispersion, the addition of poor solvents can promote better binding between additives and asphaltene, thereby enhancing the dispersion stability of asphaltene.

Fig. 9 is the IGM analysis of different additive molecules interacting with SiO_2 surface. Table 5 illustrates the interaction energies between various additive molecules and SiO_2 surface, as well as the additives' respective contributions to dispersion energy. The interaction energy between the neutral SHSn and the SiO_2 surface is −397.48 kJ/mol, whereas the interaction energy between the doubly cationic SHSc and the SiO_2 surface is −479.82 kJ/mol. The difference is not significant. In Fig. 9(b1), a strong electrostatic attraction and repulsion phenomenon can be observed between the amine groups of SHSn and the SiO_2 surface. The amine groups of SHSn demonstrates a negative ESP, which facilitates the formation of hydrogen bonds with the positively charged ESP of the hydroxyl hydrogen on the SiO_2 surface. Nevertheless, in the context of the silicon hydroxy oxygen region with negative ESP, it shows a repulsive interaction towards the SHSn amine groups. In Fig. 9(b2), SHSc acts as a cation, establishing an electrostatic attraction region with the silanol oxygen characterized by a negative ESP. However, no significant electrostatic repulsion region is identified. The hydrogen bonds between SHSn and the SiO_2 surface improve SHSn's affinity to solid surfaces. Especially, when SHSn is not inclined to encapsulate asphaltenes, it tends to spread on the solid surface. This behavior weakens the adsorption of asphaltenes on the SiO_2 surface, aligning with the findings of MD simulations and previous experimental results (Li, et al. 2011, 2016, 2018; Sui, et al. 2016, 2018; Zhang et al., 2018).

In the case of IL-CH and SHS-CH, substituting a nitrogen atom with a carbon atom decreases their interaction energies with the SiO_2 surface by −85.40 kJ/mol and −97.40 kJ/mol, respectively. This reduction is attributed to the absence of nitrogen atoms,

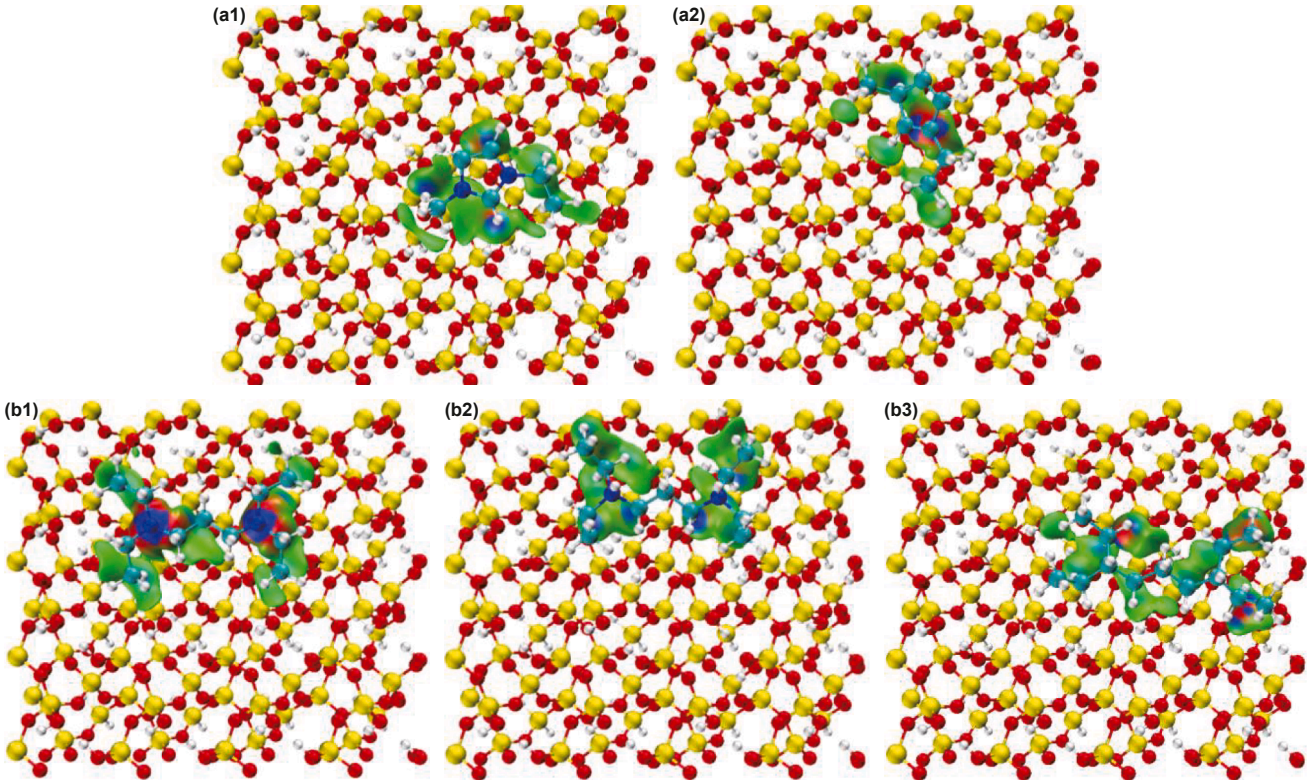

Fig. 9. IGM analysis of different additive molecules interacting with SiO_2 surface: **(a1)** ILc molecule, **(a2)** IL-CH molecule, **(b1)** SHSc molecule, **(b2)** SHSn molecule, **(b3)** SHS-CH molecule.

Table 5
Interaction energies of various additive molecules with SiO_2 surface, and additives' contributions to dispersion energy.

Additives	The interaction energies between various additive molecules and SiO_2 surface, kJ/mol	Additives' respective contributions to dispersion energy, kJ/mol
ILc	−186.27	−443.76
IL-CH	−85.40	−450.70
SHSn	−397.48	−565.17
SHSc	−479.82	−557.85
SHS-CH	−97.40	−556.47

which diminishes the ability to form strong electrostatic attractions on the solid surface and thus impairs the displacement of asphaltenes.

3.3. Mechanisms for improving extraction efficiency

Based on the above results, a clear summary of the dominant mechanism by which the additives enhance the oil–solid separations is presented in Fig. 10. A table in Supporting Information S9 summarizes the key energetic metrics used throughout the study and maps each metric to the specific conclusions it is used to support.

For ionic liquids, the ILc carries positive charges and presents positive ESP. In Fig. 10(a1), the complementary relationship between the negative ESP of fused rings in asphaltene and the positive ESP of ILc results in an electrostatic attractive interaction. Furthermore, ILc exhibits electrostatic and dispersion attraction to the solid surface of SiO_2. In addition to the small size and low resistance of ILc molecules, they exhibit a tendency to disperse and desorb aggregated asphaltenes, as shown in Fig. 10(b1). Zeta potential measurements confirm that the addition of ionic liquids will increase the positive charges of asphaltene droplets. This indicates that cations are adsorbed on the asphaltene surface (Zhang et al., 2018).

For switchable-hydrophilicity solvents, SHSc and SHSn present distinct microscopic mechanisms, illustrated in Fig. 10(a2) and (b2). SHSc, with its positive ESP, interacts with the negative ESP of the asphaltene's fused rings. The large molecular size of SHSc results in spatial hindrance that leads to a mode of interaction characterized by a stabilizing effect on the asphaltene aggregates, rather than full dispersion. This leads to partial desorption, slightly reducing the interaction between asphaltenes and the mineral surface. On the other hand, SHSn, with its negative ESP on amine groups, repels the fused rings of asphaltene while forming attractive interactions with the hydroxyl groups on the silica surface. This competition for adsorption sites between SHSn and asphaltenes on the SiO_2 surface facilitates the detachment of asphaltene aggregates and promotes their solubility in the aqueous phase. Experimental results demonstrate that the water penetration time of solids extracted with undissociated SHSn is 1350 ± 49 s. In contrast, for solids subjected to water extraction

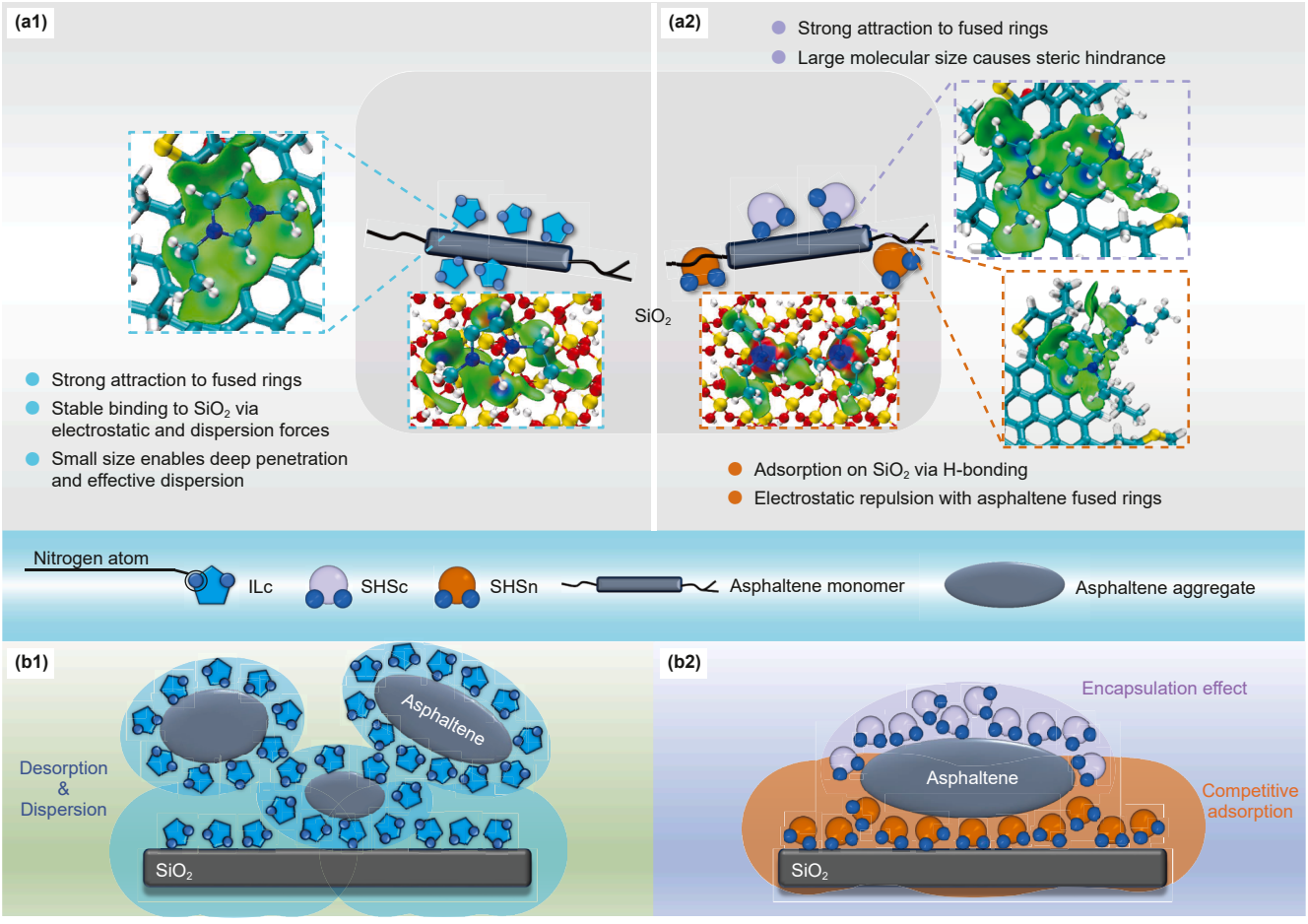

Fig. 10. **(a1)** Effects of ILc on asphaltenes and SiO_2 surfaces. **(a2)** Effects of SHSc and SHSn on asphaltenes and SiO_2 surfaces. **(b1)** Interfacial behaviors of ILc in the asphaltene–SiO_2 system. **(b2)** Interfacial behaviors of SHSc and SHSn in the asphaltene–SiO_2 system.

with SHS, which utilizes the synergistic effect of SHSn and SHSc, this time is reduced to 160 ± 8 s. This confirms that the synergistic effect of SHSn and SHSc is more conducive to the displacement and dispersion of asphaltenes from the solid surface (Li et al., 2018).

From the perspective of intermolecular interactions, the overall attractive interactions between the additives and asphaltene molecules are dominated by dispersion interactions. For organic molecules, dispersion interactions serve to establish a stable baseline affinity. However, the presence of cationic nitrogen groups introduces a significant electrostatic component, which modifies the competitive interactions at the interface. Specifically, these cationic nitrogen groups enhance electrostatic attraction and overcome exchange repulsion, thereby improving the additive molecules' ability to displace asphaltenes from solid surfaces under adsorption conditions. Thus, while dispersion interactions constitute the strongest physical mechanism of intermolecular interactions, electrostatic interactions have a critical impact on interfacial displacement and competitive adsorption behavior. The properties of the solvent significantly influence additive–asphaltene interactions by modulating binding. In poor solvents, the additive exhibits sustained association with asphaltene, reducing solvent-exposed surface area and thereby enhancing dispersion stability.

This study shows that ionic and non-ionic nitrogen-based additives enhance asphaltene desorption by modulating electrostatic interactions at mineral surfaces. Optimizing the charge properties of these additives weakens asphaltene–mineral interaction, improving desorption efficiency and reducing chemical use. The results also indicate that molecular architecture governs the balance between electrostatic displacement, hydrogen-bond competition, and potential encapsulation. Together, these findings provide a basis for designing targeted surface treatments that improve oil separation under heterogeneous field conditions with varying mineral compositions and contaminant levels, thereby enabling more efficient heavy oil recovery.

4. Conclusions

MD and DFT simulations jointly elucidate the distinct molecular mechanisms by which nitrogen-containing additives regulate asphaltene–silica interfacial interactions. ILc exhibits pronounced electrostatic and dispersion interactions with silica, together with strong π-affinity for asphaltene aromatic cores. Its compact cationic structure readily intercalates between stacked asphaltenes, substantially promoting their desorption and lowering the asphaltene–silica binding energy by 81.32%. SHSc also engages asphaltenes through cationic nitrogen centers; however, its bulky architecture induces significant steric hindrance, leading predominantly to partial encapsulation rather than effective displacement. In contrast, the bulky dicationic SHSc favors asphaltene encapsulation over displacement, while neutral SHSn relies on hydrogen-bond-mediated competitive adsorption with limited efficiency.

These findings establish a dual-function mechanism: cationic nitrogen functionalities drive intercalation via electrostatic complementarity, whereas neutral nitrogen groups act through hydrogen-bond–mediated competitive adsorption. The resulting desorption efficiency trend (ILc > SHSn > SHSc) provide guidance for additive design—prioritizing compact π-active cations, avoiding sterically hindered structures, and strategically incorporating hydrogen-bonding co-modifiers.

Although consistent with prior experimental observations, the study acknowledges limitations in system size and asphaltene representation. Future work will expand molecular architectures and validate performance across realistic mineral surfaces under reservoir conditions.

CRediT authorship contribution statement

Xue-Qian Liu: Writing – original draft, Software, Methodology, Formal analysis, Data curation. **Chang-Qing He:** Writing – original draft, Software, Methodology, Investigation, Formal analysis. **Guo-Qiang Ma:** Methodology, Investigation, Formal analysis. **Lin He:** Writing – original draft, Validation, Supervision, Project administration, Funding acquisition. **Hong Sui:** Validation, Supervision, Project administration.

Declaration of competing interest

The authors declare that they have no known competing financial interests or personal relationships that could have appeared to influence the work reported in this paper.

Acknowledgements

This work was financially supported by the National Natural Science Foundation of China (NSFC, No. 22178252). We thank the anonymous reviewers for constructive feedback that strengthened this work.

Appendix A. Supplementary data

Supplementary data to this article can be found online at https://doi.org/10.1016/j.petsci.2026.01.048.

References

Ahmadi, M., Chen, Z., 2020. Challenges and future of chemical assisted heavy oil recovery processes. Adv. Colloid Interface Sci. 275, 102081. https://doi.org/10.1016/j.cis.2019.102081.

Bai, Y., Sui, H., Liu, X., He, L., Li, X., Thormann, E., 2019. Effects of the N, O, and S heteroatoms on the adsorption and desorption of asphaltenes on silica surface: A molecular dynamics simulation. Fuel 240, 252–261. https://doi.org/10.1016/j.fuel.2018.11.135.

Bannwarth, C., Ehlert, S., Grimme, S., 2019. GFN2-xTB—An accurate and broadly parametrized self-consistent tight-binding quantum chemical method with multipole electrostatics and density-dependent dispersion contributions. J. Chem. Theor. Comput. 15 (3), 1652–1671. https://doi.org/10.1021/acs.jctc.8b01176.

Bastami, D., Shahrabadi, A., Taghikhani, V., Naderi, H., Taheri-Shakib, J., 2024. A novel method for examining the influence of molecular and structural properties of the asphaltene fraction on the wettability change of the calcite surface. Fuel 363, 130935. https://doi.org/10.1016/j.fuel.2024.130935.

Burns, L.A., Mayagoitia, A.V., Sumpter, B.G., Sherrill, C.D., 2011. Density-functional approaches to noncovalent interactions: a comparison of dispersion corrections (DFT-D), exchange-hole dipole moment (XDM) theory, and specialized functionals. J. Chem. Phys. 134 (8), 084107. https://doi.org/10.1063/1.3545971.

Celia-Silva, L.G., Vilela, P.B., Morgado, P., Lucas, E.F., Martins, L.F., Filipe, E.J., 2020. Preaggregation of asphaltenes in the presence of natural polymers by molecular dynamics simulation. Energy Fuels. 34 (2), 1581–1591. https://doi.org/10.1021/acs.energyfuels.9b03703.

Dang, C., Nghiem, L., Nguyen, N., Yang, C., Chen, Z., Bae, W., 2018. Modeling and optimization of alkaline-surfactant-polymer flooding and hybrid enhanced oil recovery processes. J. Petrol. Sci. Eng. 169, 578–601. https://doi.org/10.1016/j.petrol.2018.06.017.

Frisch, M., Trucks, G., Schlegel, H., Scuseria, G., Robb, M., Cheeseman, J., Scalmani, G., Barone, V., Mennucci, B., Petersson, G., 2010. Gaussian 09, Revision C01 Inc. Wallingford Ct.

Fu, L., Gu, F., Liao, K., Wen, X., Jiang, L., Li, X., Huang, W., Shao, M., 2022. Molecular dynamics simulation of enhancing surfactant flooding performance by using SiO_2 nanoparticles. J. Mol. Liq. 367, 120404. https://doi.org/10.1016/j.molliq.2022.120404.

Gonzalez, V., Taylor, S.E., 2016. Asphaltene adsorption on quartz sand in the presence of pre-adsorbed water. J. Colloid Interface Sci. 480, 137–145. https://doi.org/10.1016/j.jcis.2016.07.014.

He, C., Zhang, X., He, L., Sui, H., Li, X., 2022. Revealing the non-covalent interactions between oxygen-containing demulsifiers and interfacially active asphaltenes: A multi-level computational simulation. Fuel 329, 125375. https://doi.org/10.1016/j.fuel.2022.125375.

Hou, J., Du, J., Sui, H., Sun, L., 2021. Surfactants enhanced heavy oil–solid separation from carbonate asphalt rocks-experiment and molecular dynamic simulation. Nanomaterials 11 (7), 1835. https://doi.org/10.3390/nano11071835.
Humphrey, W., Dalke, A., Schulten, K., 1996. VMD: visual molecular dynamics. J. Mol. Graph. 14 (1), 33–38. https://doi.org/10.1016/0263-7855(96)00018-5.
Kuznicki, T., Masliyah, J.H., Bhattacharjee, S., 2009. Aggregation and partitioning of model asphaltenes at toluene–water interfaces: molecular dynamics simulations. Energy Fuels. 23 (10), 5027–5035. https://doi.org/10.1021/ef9004576.
Li, X., Sun, W., Wu, G., He, L., Li, H., Sui, H., 2011. Ionic liquid enhanced solvent extraction for bitumen recovery from oil sands. Energy Fuels. 25 (11), 5224–5231. https://doi.org/10.1021/ef2010942.
Li, X., Wang, J., He, L., Sui, H., Yin, W., 2016. Ionic liquid-assisted solvent extraction for unconventional oil recovery: Computational simulation and experimental tests. Energy Fuels. 30 (9), 7074–7081. https://doi.org/10.1021/acs.energyfuels.6b01291.
Li, X., Yang, Z., Sui, H., Jain, A., He, L., 2018. A hybrid process for oil-solid separation by a novel multifunctional switchable solvent. Fuel 221, 303–310. https://doi.org/10.1016/j.fuel.2018.02.081.
Liu, F., Hickman, S., Maqbool, T., Pauchard, V., Banerjee, S., 2020. Study of asphaltene deposition onto stainless-steel surfaces using quartz crystal microbalance with dissipation. Energy Fuels. 34 (8), 9283–9295. https://doi.org/10.1021/acs.energyfuels.0c00663.
Liu, F., Yang, H., Wang, J., Qian, Y., Wu, J., Li, S., Liu, Q., Yang, S., Xu, S., Zhang, X., 2019. Molecular interaction between asphaltene and quartz with different surface wettability: A combined study of experimental measurement and theoretical calculation. Fuel 258, 115937. https://doi.org/10.1016/j.fuel.2019.115937.
Lu, T., 2025. Version 1.0 (Dev5). (Accessed 28 February 2025). http://sobereva.com/soft/Sobtop.
Lu, T., Chen, F., 2012. Multiwfn: a multifunctional wavefunction analyzer. J. Comput. Chem. 33 (5), 580–592. https://doi.org/10.1002/jcc.22885.
Lu, Y., Li, R., Manica, R., Liu, Q., Xu, Z., 2021. Enhancing oil–solid and oil–water separation in heavy oil recovery by CO-responsive surfactants. AIChE J. 67 (1), e17033. https://doi.org/10.1002/aic.17033.
Martínez, L., Andrade, R., Birgin, E.G., Martínez, J.M., 2009. PACKMOL: a package for building initial configurations for molecular dynamics simulations. J. Comput. Chem. 30 (13), 2157–2164. https://doi.org/10.1002/jcc.21224.
Melendez-Alvarez, A.A., Garcia-Bermudes, M., Tavakkoli, M., Doherty, R.H., Meng, S., Abdallah, D.S., Vargas, F.M., 2016. On the evaluation of the performance of asphaltene dispersants. Fuel 179, 210–220. https://doi.org/10.1016/j.fuel.2016.03.056.
Mohammed, I., Al-Shehri, D., Mahmoud, M., Sultan, A.S., Kamal, M.S., Alade, O., Elsayed, M., Adebayo, A.R., Patil, S., 2024. Evaluation of polymers as a strategy to reduce asphaltene adsorption on rock surface. SPE J. 29 (1), 215–231. https://doi.org/10.2118/213613-PA.
Montoya, T., Coral, D., Franco, C.A., Nassar, N.N., Cortés, F.B., 2014. A novel solid–liquid equilibrium model for describing the adsorption of associating asphaltene molecules onto solid surfaces based on the “chemical theory”. Energy Fuels. 28 (8), 4963–4975. https://doi.org/10.1021/ef501020d.
Natarajan, A., Kuznicki, N., Harbottle, D., Masliyah, J., Zeng, H., Xu, Z., 2014. Understanding mechanisms of asphaltene adsorption from organic solvent on mica. Langmuir 30 (31), 9370–9377. https://doi.org/10.1021/la500864h.
Niu, J., Liu, Q., Lv, J., Peng, B., 2020. Review on microbial enhanced oil recovery: Mechanisms, modeling and field trials. J. Petrol. Sci. Eng. 192, 107350. https://doi.org/10.1016/j.petrol.2020.107350.
Oostenbrink, C., Villa, A., Mark, A.E., Van Gunsteren, W.F., 2004. A biomolecular force field based on the free enthalpy of hydration and solvation: the GROMOS force-field parameter sets 53A5 and 53A6. J. Comput. Chem. 25 (13), 1656–1676. https://doi.org/10.1002/jcc.20090.
Pratama, R.A., Babadagli, T., 2022. A review of the mechanics of heavy-oil recovery by steam injection with chemical additives. J. Petrol. Sci. Eng. 208, 109717. https://doi.org/10.1016/j.petrol.2021.109717.
Razavinezhad, J., Jafari, A., Elyaderani, S.M.G., 2022. Experimental investigation of multi-walled carbon nanotubes assisted surfactant/polymer flooding for enhanced oil recovery. J. Petrol. Sci. Eng. 214, 110370. https://doi.org/10.1016/j.petrol.2022.110370.
Saeedi Dehaghani, A.H., Behnam Motlagh, M.A., 2025. Experimental investigation of foam stability under various salinity levels, oil types, and surfactant conditions: effect of natural polymer lignin. Sci. Iran. https://doi.org/10.24200/sci.2025.66165.9885.
Stratiev, D., Nikolova, R., Veli, A., Shishkova, I., Toteva, V., Georgiev, G., 2025. Mitigation of asphaltene deposit formation via chemical additives: A review. Processes 13 (1), 141. https://doi.org/10.3390/pr13010141.
Sui, H., Ma, G., Yuan, Y., Li, Q., He, L., Wang, Y., Li, X., 2018. Bitumen-silica interactions in the presence of hydrophilic ionic liquids. Fuel 233, 860–866. https://doi.org/10.1016/j.fuel.2018.06.114.
Sui, H., Xu, L., Li, X., He, L., 2016. Understanding the roles of switchable-hydrophilicity tertiary amines in recovering heavy hydrocarbons from oil sands. Chem. Eng. J. 290, 312–318. https://doi.org/10.1016/j.cej.2016.01.056.
Taheri-Shakib, J., Esfandiarian, A., Rajabi-Kochi, M., Kazemzadeh, E., Afkhami Karaei, M., 2024. Evaluation of rock and fluid intermolecular interaction between asphaltene and sand minerals using electrochemical, analytical spectroscopy and microscopy techniques. Sci. Rep. 14 (1), 670. https://doi.org/10.1038/s41598-024-51196-3.
Tazikeh, S., Shafiei, A., Yerkenov, T., Abenov, A., Seitmaganbetov, N., Atabaev, T.S., 2022. A systematic and critical review of asphaltene adsorption from macroscopic to microscopic scale: Theoretical, experimental, statistical, intelligent, and molecular dynamics simulation approaches. Fuel 329, 125379. https://doi.org/10.1016/j.fuel.2022.125379.
Vatti, A.K., Divi, S., Dey, P., 2024. Effectiveness of inhibitors to prevent asphaltene aggregation: Insights from atomistic and molecular simulations. J. Chem. Phys. 160 (9), 090901. https://doi.org/10.1063/5.0190779.
Xiong, Y., Cao, T., Chen, Q., Li, Z., Yang, Y., Xu, S., Yuan, S., Sjoblom, J., Xu, Z., 2017. Adsorption of a polyaromatic compound on silica surfaces from organic solvents studied by molecular dynamics simulation and AFM imaging. J. Phys. Chem. C 121 (9), 5020–5028. https://doi.org/10.1021/acs.jpcc.6b11763.
Yang, D., Peng, X., Peng, Q., Wang, T., Qiao, C., Zhao, Z., Gong, L., Liu, Y., Zhang, H., Zeng, H., 2022. Probing the interfacial forces and surface interaction mechanisms in petroleum production processes. Engineering 18, 49–61. https://doi.org/10.1016/j.eng.2022.06.012.
Yang, Y., Sui, H., Ma, J., He, L., Li, X., 2021. Revealing the residual mechanism of switchable solvents in heavy oil. Fuel Process. Technol. 218, 106857. https://doi.org/10.1016/j.fuproc.2021.106857.
Zhang, J., Gao, H., Xue, Q., 2020. Potential applications of microbial enhanced oil recovery to heavy oil. Crit. Rev. Biotechnol. 40 (4), 459–474. https://doi.org/10.1080/07388551.2020.1739618.
Zhang, X., Wang, J., Zhang, X., He, L., Sui, H., Li, X., 2023. Stability of asphaltene-mircoparticles co-stabilized emulsions by oxygen-enriched nonionic demulsifier. J. Mol. Liq. 381, 121819. https://doi.org/10.1016/j.molliq.2023.121819.
Zhang, Z., Kang, N., Wang, J., Sui, H., He, L., Li, X., 2018. Synthesis and application of amino acid ionic liquid-based deep eutectic solvents for oil-carbonate mineral separation. Chem. Eng. Sci. 181, 264–271. https://doi.org/10.1016/j.ces.2018.02.023.
Zhou, W., Tang, X., Liu, X., Yan, Y., Chen, C., 2024. Interfacial behaviors and oil detachment mechanisms by modified silica nanoparticles: insights from molecular simulations. J. Phys. Chem. B. 128 (12), 2985–2994. https://doi.org/10.1021/acs.jpcb.3c07697.